Published in final edited form as:
J Magn Reson Imaging. 2010 July ; 32(1): 242–248. doi:10.1002/jmri.22204.

Reduced FOV Single-Shot Fast Spin Echo Imaging Using Two-dimensional Spatially-Selective RF Pulses

Jing Yuan, PhD[1,*], **Tzu-Cheng Zhao, PhD**[2], **Yi Tang, MD**[3], and **Lawrence P. Panych, PhD**[3]

[1]Department of Diagnostic Radiology and Organ Imaging, The Chinese University of Hong Kong, Shatin, New Territories, Hong Kong, China

[2]Department of Electronic Engineering, National Taiwan University, Taipei, Taiwan

[3]Department of Radiology, Brigham and Women's Hospital, Harvard Medical School, Boston, MA, USA

Abstract

Purpose—To demonstrate reduced field-of-view (RFOV) single-shot fast spin echo (SS-FSE) imaging based on the use of two-dimensional spatially-selective RF pulses.

Materials and Methods—2DRF pulses were incorporated into a SS-FSE sequence for RFOV imaging in both phantoms and the human brain on a 1.5 T whole-body MR system with the aim of demonstrating improvements in terms of shorter scan time, reduced blurring and higher spatial resolution compared to full FOV imaging.

Results—For phantom studies, scan time gains of up to 4.2 fold were achieved as compared to the full FOV imaging. For human studies, the spatial resolution was increased by a factor of 2.5 (from 1.7 mm/pixel to 0.69 mm/pixel) for RFOV imaging within a scan time (0.7s) similar to full FOV imaging. A 2.2-fold shorter scan time along with a significant reduction of blurring was demonstrated in RFOV images compared to full FOV images for a target spatial resolution of 0.69 mm/pixel.

Conclusion—RFOV SS-FSE imaging using a 2DRF pulse shows advantages in scan time, blurring, and SAR reduction along with true spatial resolution increase compared to full FOV imaging. This approach is promising to benefit fast imaging applications such as image guided therapy.

Keywords

reduced field-of-view imaging; single-shot fast spin echo; 2DRF pulse; echo train length; blurring; echo spacing

INTRODUCTION

Fast spin echo (FSE), or turbo spin echo (TSE), and rapid acquisition with relaxation enhancement (RARE), are important fast imaging sequences that employ an RF excitation pulse followed by a number of refocusing pulses in an echo-train to produce multiple spin echoes (1). With single-shot FSE (SS-FSE), all *k*-space lines needed for image reconstruction are collected in one acquisition so that imaging time can be even further reduced. However, the extremely long echo-train length (ETL) in SS-FSE has side effects

[*]Department of Diagnostic Radiology and Organ Imaging, The Chinese University of Hong Kong, Shatin, New Territories, Hong Kong, China jyuan@cuhk.edu.hk Tel: 852-2632-1036 Fax: 852-2636-0012.

that result in a degradation of image quality. Firstly, severe blurring usually occurs along the phase-encoding (PE) direction as a result of T_2-induced signal decay during the echo train acquisition. Secondly, spatial resolution is sometimes sacrificed in order to reduce the effects of the T_2-induced signal decay. Other problems associated with SS-FSE include edge enhancement, ghosting, and a higher specific absorption rate (SAR).

Reduction of the total echo-train duration could be accomplished by either shortening the echo spacing (ESP) or reducing the ETL. Many strategies, such as increasing the receiver bandwidth, using maximum slew rate, and minimizing the refocusing RF pulse duration, can be used to shorten the ESP. However, even with these modifications, the reduction of the echo train duration may still be insufficient for tissues with short T_2 values.

Reduced field-of-view (RFOV) imaging (2-5) along the PE direction can be employed to reduce the number of k_y lines and hence reduce the ETL without sacrificing spatial resolution for those applications in which only a small portion of the FOV may be of clinical interest.

Several techniques have been demonstrated for RFOV imaging, including: spatial pre-saturation (6,7), orthogonal RF excitation (8-10) and two-dimensional spatially-selective RF (2DRF) pulses (5,11-14). In the spatial pre-saturation technique, pre-saturation RF pulses are used to excite the longitudinal spins into the transverse plane within desired saturation regions, and are followed by spoiler gradient pulses to dephase the transverse magnetization. The normal imaging sequence is then played out after the transverse magnetization in the saturation regions has been dephased. Compared to the use of a 2DRF pulse, spatial pre-saturation is usually much more sensitive to B_1 inhomogeneity, although some techniques have been employed to improve the B_1 inhomogeneity tolerance (15-17). For pulse sequences with long *TR* such as SS-FSE, another problem associated with spatial pre-saturation is that T_1 recovery of the transverse magnetization in the saturation region during acquisition usually degrades saturation performance. When using 2DRF pulses there is no such T_1 recovery problem because the spins outside of the region-of-interest (ROI) are never excited. Another option is orthogonal RF excitation, where the slice selection gradient for the excitation 90-degree pulse is orthogonal to a selection gradient for the 180-degree refocusing pulse so that the intersection of these two selection profiles produces the desired *RFOV* excitation profile. Orthogonal RF excitation is only compatible with spin-echo sequences. A further limitation of the orthogonal excitation approach is that dark saturation bands result when the technique is used for multi-slice acquisitions. Compared to the previous two RFOV methods, using 2DRF pulses can be an efficient solution for RFOV imaging. To the best of our knowledge, 2DRF pulses for RFOV imaging have been proposed for echo-planar imaging (EPI) (11,13,14), normal gradient echo sequences (5,12), but have not been applied for SS-FSE. The use of 2DRF pulses for RFOV SS-FSE for reduction of scan time, SAR and blurring is the focus of the work reported in this paper.

MATERIALS AND METHODS

2DRF Pulse Design

The echo-planar 2DRF pulse design used in this work is based on the theory presented by Pauly *et al* in 1989 (12). A rectangular path in excitation k-space in the shape of an echo planar trajectory is applied to provide independent excitation slice thickness control along both slice selection direction (*z*) and the phase encoding direction (*y*). The waveform for a 9-subpulse echo-planar 2DRF pulse is shown in Fig. 1(a) and the corresponding excitation profile is plotted in Fig. 1(b). The RF waveform contains a train of SINC-type sub-pulses with durations of T_{sub}. The amplitude for each sub-pulse is weighted by a SINC-Hamming modulation envelope. The sub-pulses can be played out either during *Gz* slice-selective

gradients that are both positive and negative (the bi-polar mode) or only during a positive-only *Gz* (the fly-back mode). Gradient waveforms *Gy* along the PE direction are composed of short blips at the end of each sub-pulse, with the last blip to bring the trajectory back to excitation *k*-space center. If the SINC-Hamming envelope has zero-crossings as shown in Fig. 1(a), the corresponding sub-pulse will have zero weighting and can be neglected with minimal impact on the resulting spatial excitation profile. In this case, the areas for the corresponding *Gy* blips are doubled (18).

Through applying the Nyquist theorem to an analysis in excitation *k*-space, it can be seen that the 2DRF excitation profile is replicated periodically along the PE direction (*y*) as shown in Fig.1(b). The distance between two neighboring excitation replicates, or the field of excitation (FOE), is determined by the blip area (a_{blip}) with the relationship of $FOE = 2\pi/\gamma a_{blip}$, where γ is the gyromagnetic ratio. Subpulse density D_s, which is defined by the total number of subpulses divided by the time-bandwidth product (TBW) of the envelope pulse, determines the size ratio of the excited region (or passband width, W_p, including the plateau and the transition region) to the unexcited region (or stopband width, W_s). The sum of passband width and stopband width equals the *FOE* size. The more subpulses in each cycle of modulation envelop, the smaller is the value of W_p/W_s.

The 2DRF pulse was programmed to produce subpulses dynamically in the sequence, replacing the 90° excitation pulse by prescribing the sub-pulse duration, number of sub-pulses, the cycles of the SINC-Hamming modulation envelope and the FOE on the scanner console for each scan. Our approach differs programmatically from other studies where a pre-defined static 2DRF waveform is inserted into the sequence with a fixed excitation size (11,13,14). This dynamic 2DRF pulse programming approach provides more flexibility for applications requiring different sizes of ROIs without the need to design a new 2DRF pulse waveform for each scan. For the imaging experiments in this study, a bi-polar 2DRF pulse with seven subpulses (688μs each, 4.8ms in total) was used to achieve a reduction factor up to five. All subpulses are within the main lobe of the SINC-Hamming envelope.

Imaging Experiments

Experiments were performed on a GE Signa 1.5*T* scanner (General Electric Medical Systems, Milwaukee,WI) with echo-speed gradients (40 *mT* /*m* maximum gradient strength and a maximum slew rate of 150 *T* / *m*/ *s*) and a standard quadrature head coil. A product half-Fourier acquired single-shot turbo spin echo (HASTE) was adapted for SS-FSE imaging. Half of the full k_y lines plus six overscan k_y lines at negative low spatial frequency in *k*-space were acquired.

In the phantom study, an ACR (American College of Radiology) phantom was scanned. This phantom is filled with 10 millimolar (mmol) nickel chloride solution containing sodium chloride (45 mmol) to simulate biological conductivity. Both full FOV and RFOV images were acquired with common imaging parameters of FOV = 22 cm, matrix = 256×256, slice thickness = 8 mm, receiver bandwidth = 83.33 kHz. For human studies, head images of two healthy subjects were acquired under an approved Institutional Review Board protocol. Receiver bandwidth of 20.83 kHz, FOV of 22 cm and slice thickness of 5 mm were used. In the sagittal plane, the PE direction was chosen as posterior-to-anterior (P-A). High spatial resolution RFOV images (320×320) were demonstrated and compared to the full FOV images (128×128 and 192×192). In the axial plane, the PE direction was posterior-to-anterior (P-A). All images were acquired with high resolution of 320 × 320 within a 22 cm FOV. The FOV reduction factor (RFOV) of two was used to demonstrate the blurring reduction compared to full FOV images.

RESULTS

Fig. 2(a) shows a full FOV image obtained by using the original product slice-selective RF pulse. Fig. 2(b-e) demonstrates the corresponding RFOV images with reduction factor from two to five by the 2DRF pulse respectively. Corresponding imaging parameters are listed in Table. 1 for comparison. Prominent blurring can be found in Fig. 2(a) along the vertical grid lines compared to the horizontal grid lines due to T_2 decay during the long echo train acquisition. By contrast, the blurring artifact is significantly reduced in RFOV images, as seen in Figs. 2(b-e). The minimum *TR* was significantly reduced from 1.8 *s* for full FOV image to 0.43 *s* for the RFOV image with the FOV reduction factor of five.

A comparison of the full FOV images of an ACR phantom with those RFOV images (R_{FOV}=4) using different matrix sizes and receiver bandwidths is shown in Fig. 3. The *TR*s for full FOV images (a-d) with matrix size of 256×256 and 448×448 were 1797 *ms* and 3925 *ms* respectively regardless of receiver bandwidth. For RFOV images shown in Figs. 3(e-h), the TRs were reduced to 511 *ms* and 1058 *ms* correspondingly for matrix size of 256 ×256 and 448×448.

Fig. 4 shows a comparison in spatial resolution between full FOV and RFOV for *in vivo* head images. Matrix sizes of 128 × 128 and 192 × 192 were acquired for Fig. 4(a) and (b), respectively. Matrix sizes of 320 ×320 with R_{FOV} of two and three were used for Fig. 4(c) and (d), respectively. The total scan times for Fig. 4(a-d) were 0.74 s, 1.22 s, 0.94 s and 0.69 s, respectively. Compared to full FOV images, fine structures in cerebellum can be seen in RFOV images due to the much higher spatial resolution. Note that these images have different T2 contrast due to the different effective TEs. The longer duration of the 2DRF pulse compared to the product RF pulse, and the longer duration of the readout gradient (required for higher resolution), both contribute to the extended TE and give greater T2-weighting in the RFOV images.

Fig. 5 demonstrates the reduction of blurring in a local-look RFOV image (Fig.5(c)) compared to a full FOV image (Fig.5(b)) with the same spatial resolution of 320×320. In Fig. 5(b), the septum pellucidum and fornix, (indicated by the white arrow), are blurred due to the T_2 decay over the long echo train duration. These fine structures, however, when seen in the RFOV image of Fig. 5(b), are better visualized as a result of the echo train length being halved. For the same reason, the internal cerebral veins (indicated by the yellow arrow), show less blurring in the RFOV image.

DISCUSSION

In this study, RFOV SS-FSE imaging using echo-planar 2DRF pulses was demonstrated to reduce scan time, increase spatial resolution and improve blurring. Scan time gains of up to 4.2 fold were achieved as compared to the full FOV imaging for phantom studies. For human studies, the spatial resolution was increased by a factor of 2.5 (from 1.7 mm/pixel to 0.69 mm/pixel) for RFOV imaging within a scan time (0.7s) similar to full FOV imaging. A 2.2-fold shorter scan time along with a significant reduction of blurring was also demonstrated in RFOV brain images compared to full FOV images for a target spatial resolution of 0.69 mm/pixel.

For RFOV imaging, it is required that the excitation passband width be larger than the size of the ROI. More accurately, the plateau of the passband (W_{pl}) should be larger than the size of the ROI. Otherwise the signal drop within the transition region (W_{tr}) may cause substantial signal intensity variations through the ROI. Another prerequisite for RFOV imaging by 2DRF is that no side excitation should be within the FOV, *i.e*, $FOV \leq W_p + 2W_s = W_{pl} + 2W_{tr} + 2W_s$, to avoid any signal aliasing, provided that the main excitation passband

is at the center of FOV. Theoretically, the maximum reduction factor could be expressed by $R_{FOV} = (W_p + 2W_s)/W_p = 1+ 2W_s/W_p$. As described previously, W_s/W_p is determined by the subpulse density D_s. Therefore, the more subpulses, the larger reduction factor that can be achieved. On the other hand, in order to reduce the signal drop within the transition region, the passband profile needs to be as sharp as possible. However, this requires additional cycles of the modulation envelope, which significantly increases the subpulse number and total pulse duration.

For gradient echo sequences, the minimum TE and TR will increase by $0.5T_{2DRF}$-T_{normal} and T_{2DRF}-T_{normal} respectively due to the use of a 2DRF pulse, where T_{2DRF} and T_{normal} are the total duration of the 2DRF pulse and the normal slice-selective RF pulse, respectively. However, for the SS-FSE sequence, the minimum spacing between the 90° excitation pulse and the first 180° refocusing pulse ($ESP_{90\text{-}180\text{-}min}$) will increase by $0.5T_{2DRF}$-T_{normal}, hence the ESP increase will be T_{2DRF}-$2T_{normal}$. The increase of the minimum ESP propagates through the long ETL that the minimum TR will increase significantly by $(T_{2DRF}\text{-}2T_{normal})*ETL$, provided that $2\times ESP_{90\text{-}180\text{-}min}$ is longer than the minimum spacing between two consecutive 180° refocusing pulses ($ESP_{180\text{-}180\text{-}min}$). Note that $ESP_{180\text{-}180\text{-}min}$ is determined by the durations for the *x* readout gradient pulse, 180° refocusing pulses and their crusher gradient sets. In order to reduce the scan time for RFOV imaging by the use of 2DRF pulse, the time reduction due to the shorter ETL must counteract the ESP lengthening due to the long 2DRF pulse. Otherwise, the total scan time will be increased rather than decreased by the use of a 2DRF pulse. On the other hand, if the ESP is primarily determined by the minimum spacing between two consecutive 180° refocusing pulses, *i.e.* $ESP_{180\text{-}180\text{-}min} \geq 2\times ESP_{90\text{-}180\text{-}min}$, the use of 2DRF will always gives shorter scan time for SS-FSE, even if the 2DRF pulse is longer than the normal 90° slice-selective pulse.

Spatial resolution, blurring, SNR and scan time are usually conflicting factors in SS-FSE imaging, thus tradeoffs have to be made according to the application. In general, the higher x resolution prolongs the readout gradient length and hence the ESP. Also, the higher *y* resolution lengthens the ETL. Both result in the increase of scan time and prominent blurring in the image. Because the SNR is inversely proportional to the square of matrix size, the SNR decreases significantly with the increase of spatial resolution for the same FOV. Although the low SNR could be compensated by a narrower receiver bandwidth, the blurring becomes more severe because the narrower receiver bandwidth also prolongs the readout gradient and hence the ESP, as shown in Fig. 3(d). By contrast, finding a suitable compromise between spatial resolution, SNR, blurring and scan time is possible with RFOV imaging, as demonstrated by Fig. 3(h) when compared to Fig. 3(d).

The reduction of the 2DRF pulse duration not only benefits RFOV SS-FSE imaging for scan time reduction but is also important in terms of susceptibility tolerance. In order to reduce the 2DRF pulse duration, the bi-polar mode is necessary since it has nearly double time efficiency when compared to the fly-back mode. However, even with the use of bi-polar mode 2DRF pulses to shorten the overall pulse duration, good shimming performance can be critical to compensate for B_0 inhomogeneity, especially for higher field strengths. For example, the bending at the edge of excitation profile due to the field inhomogeneity, as shown in Fig. 2 and Fig. 3, would reduce the maximum achievable FOV reduction factor. On the other hand, a delay of even a few microseconds between RF and gradient waveforms may also result in prominent half-FOV ghosts for off-center slices when using bi-polar mode 2DRF pulses (19). Therefore, a calibration procedure for bi-polar mode 2DRF pulses is often required. Calibration methods suggested in the literatures (19,20) can be employed for this purpose.

Finally, it is worth noting that the modulation envelope profile of a 2DRF pulse also acts as a spectral selective pulse. Off-resonance spins, such as fat at 220 *Hz* below water resonance (at 1.5 *T*), which are located in the spectral bandwidth of the 2DRF pulse modulation envelope, will be excited along with the on-resonance spin but with an attenuated magnitude. Along with this magnitude attenuation, a spatial shift along the PE direction will also be experienced by the off-resonance spins, depending on the subpulse number and duration, modulation envelope cycle and off-resonance frequency (21). Incompletely suppressed off-resonance signal may be aliased into the FOV, as shown by the residual fat signals (white arrows) and susceptibility (yellow arrows) in Fig. 4(c) and (d). This may be not problematic for the RFOV images as long as the aliased off-resonance signal does not overlap with the ROI. For applications where fat has to be suppressed, a longer 2DRF pulse such as the 18ms 2DRF pulse as described by Saritas *et al.* can be used (13).

In conclusion, reduced FOV imaging using echo planar 2DRF pulses has been developed for high spatial resolution SS-FSE imaging with reduced acquisition time, SAR and blurring artifact in both phantom and human studies. Unlike spatial pre-saturation and orthogonal excitation, RFOV imaging by 2DRF is less sensitive to B_1 inhomogeneity, experiences no T_1 recovery within the saturation band, and can be used for multi-slice acquisitions. These advantages make the technique promising for fast imaging applications and image-guided therapy without sacrificing image quality.

Acknowledgments

Contract grant sponsor: NIH grant U41RR019703 Running title: Reduced FOV SS-FSE Imaging with 2DRF

REFERENCES

1. Hennig J, Nauerth A, Friedburg H. RARE imaging: a fast imaging method for clinical MR. Magn Reson Med. 1986; 3(6):823–833. [PubMed: 3821461]
2. Hardy CJ, Cline HE. Spatial Localization in 2 Dimensions Using Nmr Designer Pulses. Journal of Magnetic Resonance. 1989; 82(3):647–654.
3. Jeong EK, Kim SE, Guo JY, Kholmovski EG, Parker DL. High-resolution DTI with 2D interleaved multislice reduced FOV single-shot diffusion-weighted EPI (2D ss-rFOV-DWEPI). Magnet Reson Med. 2005; 54(6):1575–1579.
4. Wilm BJ, Svensson J, Henning A, Pruessmann KP, Boesiger P, Kollias SS. Reduced field-of-view MRI using outer volume suppression for spinal cord diffusion imaging. Magnet Reson Med. 2007; 57(3):625–630.
5. Zhao L, Madore B, Panych LP. Reduced field-of-view MRI with two-dimensional spatially-selective RF excitation and UNFOLD. Magnet Reson Med. 2005; 53(5):1118–1125.
6. Felmlee JP, Ehman RL. Spatial Presaturation - a Method for Suppressing Flow Artifacts and Improving Depiction of Vascular Anatomy in Mr Imaging. Radiology. 1987; 164(2):559–564. [PubMed: 3602402]
7. Edelman RR, Atkinson DJ, Silver MS, Loaiza FL, Warren WS. Frodo Pulse Sequences - a New Means of Eliminating Motion, Flow, and Wraparound Artifacts. Radiology. 1988; 166(1):231–236. [PubMed: 3336685]
8. Mansfield P, Ordidge RJ, Coxon R. Zonally Magnified EPI in Real-Time by NMR. J Phys E Sci Instrum. 1988; 21(3):275–280.
9. Turner R, Vonkienlin M, Moonen CTW, Vanzijl PCM. Single-Shot Localized Echo-Planar Imaging (Steam Epi) at 4.7 Tesla. Magnet Reson Med. 1990; 14(2):401–408.
10. Duong TQ, Yacoub E, Adriany G. High-resolution, spin-echo BOLD, and CBF fMRI at 4 and 7 T. Magn Reson Med. 2002; 48(4):589–593. al e. [PubMed: 12353274]
11. Rieseberg S, Frahm J, Finsterbusch F. Two-dimensional spatially-selective RF excitation pulses in echo-planar Imaging. Magnet Reson Med. 2002; 47(6):1186–1193.

12. Pauly J, Nishimura D, Macovski A. A K-Space Analysis of Small-Tip-Angle Excitation. J Magn Reson. 1989; 81(1):43–56.
13. Saritas EU, Cunningham CH, Lee JH, Han ET, Nishimura DG. DWI of the spinal cord with reduced FOV single-shot EPI. Magnet Reson Med. 2008; 60(2):468–473.
14. Finsterbusch J. High-resolution diffusion tensor imaging with inner field-of-view EPI. J Magn Reson Imaging. 2009; 29(4):987–993. [PubMed: 19306448]
15. Shungu DC, Glickson JD. Sensitivity and Localization Enhancement in Multinuclear in-Vivo Nmr-Spectroscopy by Outer Volume Presaturation. Magnet Reson Med. 1993; 30(6):661–671.
16. Luo Y, de Graaf RA, DelaBarre L, Tannus A, Garwood M. BISTRO: an outer-volume suppression method that tolerates RF field inhomogeneity. Magn Reson Med. 2001; 45(6):1095–1102. [PubMed: 11378888]
17. Singh S, Rutt BK, Napel S. Projection Presaturation .2. Single-Shot Localization of Multiple Regions of Interest. J Magn Reson. 1990; 90(2):313–329.
18. Bernstein, MA.; King, KF.; Zhou, XJ. Handbook of MRI pulse sequences. Academic Press; Amsterdam ; Boston: 2004.
19. Zur Y. Design of improved spectral-spatial pulses for routine clinical use. Magnet Reson Med. 2000; 43(3):410–420.
20. Oelhafen M, Pruessmann KP, Kozerke S, Boesiger P. Calibration of echo-planar 2D-selective RF excitation pulses. Magnet Reson Med. 2004; 52(5):1136–1145.
21. Alley MT, Pauly JM, Sommer FG, Pelc NJ. Angiographic imaging with 2D RF pulses. Magnet Reson Med. 1997; 37(2):260–270.

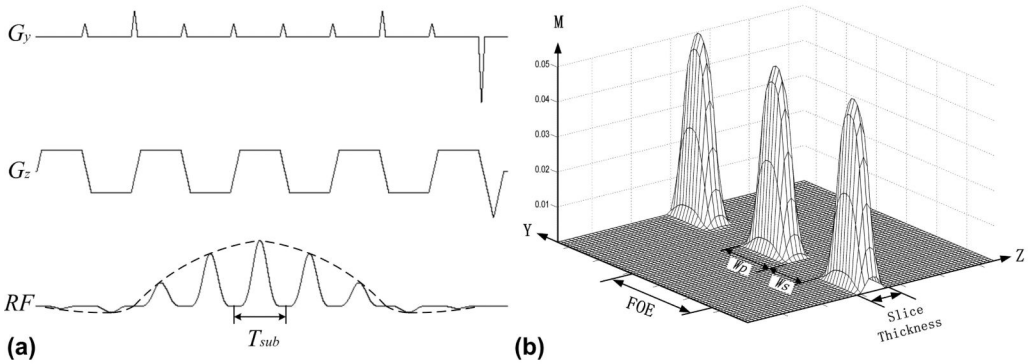

Fig. 1.

(a) RF and gradient waveforms of a bi-polar mode echo-planar 2DRF pulse. Amplitudes for RF subpulses are modulated by a SINC- Hamming envelope. Note that at the zero crossings of the modulation envelope, the sub-pulses are skipped and the blip gradient area is doubled. (b) Simulated excitation profiles by the 2DRF pulse as shown in (a). The 2DRF pulse provides independent control of excitation thickness along Y and Z directions. The FOE is determined by the G_y blip gradient area. Due to the discrete sampling of excitation k-space in the k_y direction, replicates of the excitation pattern occur periodically along the PE direction.

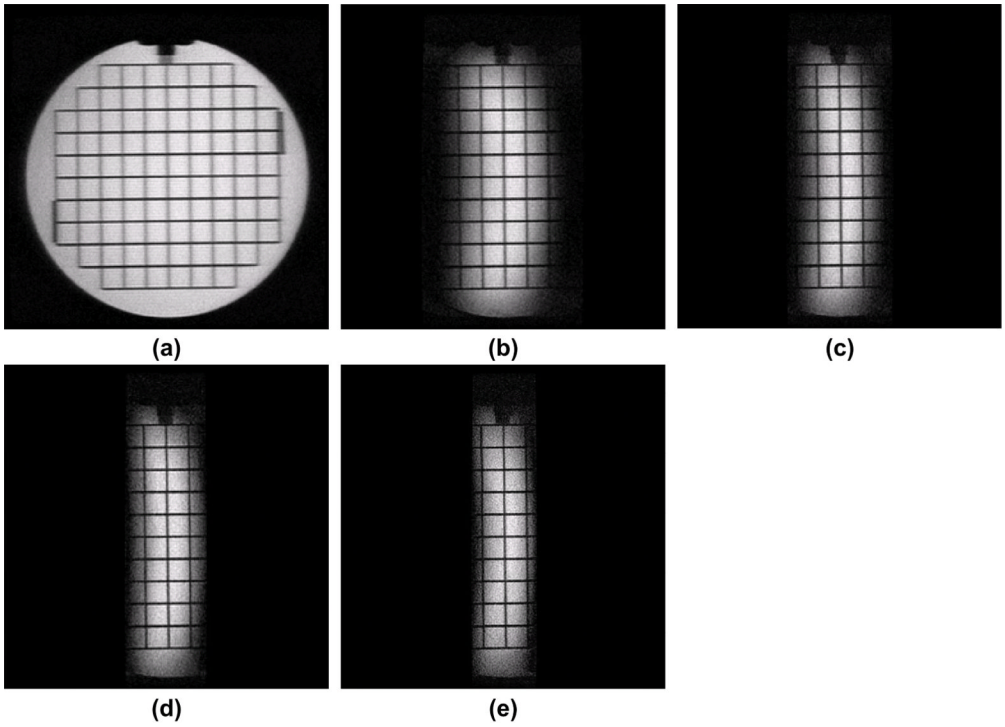

Fig. 2.

Reduced field-of-view (RFOV) ACR phantom images obtained using a 7-subpulse 2DRF pulse (FOV = 22 cm, matrix = 256 × 256, slice thickness = 8 mm, receiver bandwidth = 83.33 KHz). The subpulse duration is 688 μs. Fig. 2(a) shows a full FOV image obtained using the original slice-selective RF pulse. Figs. 2(b-e) show the RFOV images with reduction factor from two to five, respectively. The echo train length and scan time are significantly reduced without reducing spatial resolution.

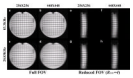

Fig. 3.
In full FOV images (a-d), the increase of resolution reduces SNR. Although the low SNR can be compensated by a narrower receiver bandwidth, this lengthens the echo spacing and hence makes the blurring more severe, as seen in Fig.3d. Using RFOV imaging (e-h), the blurring artifact is significantly reduced as demonstrated in Fig. 3h compared to Fig. 3d due to a much shorter echo train length.

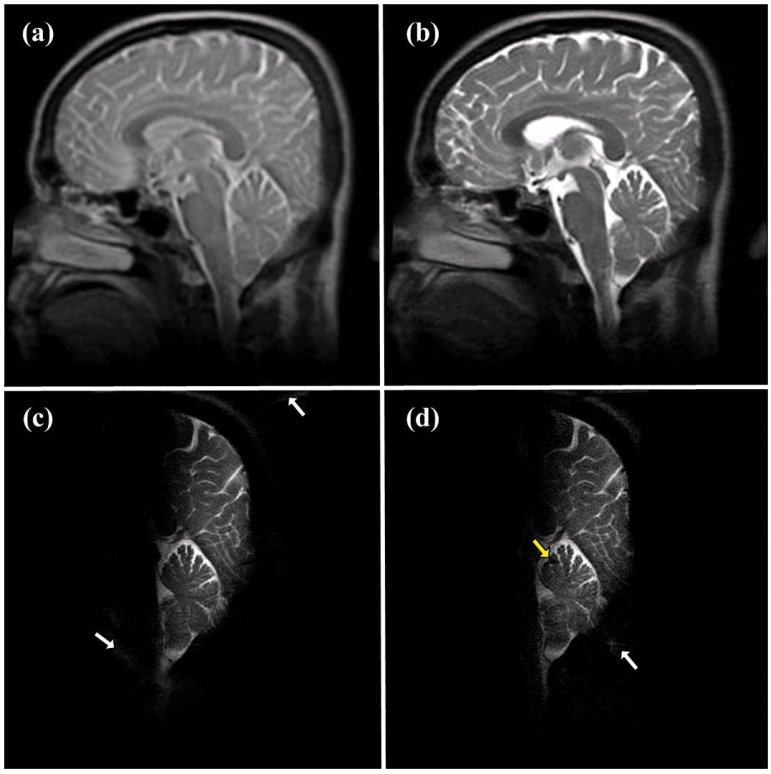

Fig. 4.

(a) Full FOV sagittal head image with 128× 128 matrix size and ETL=70; (b) full FOV sagittal head image with 192 × 192 matrix size and ETL=102; (c) RFOV sagittal head image (R_{FOV}=2) with 320 × 320 matrix size and ETL=86; (d) RFOV sagittal head image (R_{FOV}=3) with 320× 320 matrix size and ETL=66; Acquisition times for (a-d) were 0.74 *s*, 1.22 *s*, 0.94 *s* and 0.69 *s*, respectively. Note that the different effective *TE*s result in altered image contrast. The effective *TE*s were 40 ms, 53 ms, 78 ms and 78 ms for (a-d), respectively.

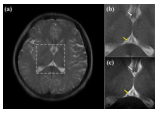

Fig. 5.

(a) A full FOV axial head image. ETL=166, *TE*=78 ms, *TR*=2.2 s, FOV=22 cm, matrix size = 320×320 and receiver bandwidth = 20.83 *KHz*; (b) A zoomed image of the ROI shown in the white square in (a); (c) The RFOV image of the same ROI with the same matrix size and receiver bandwidth. ETL=86, *TE*=81 *ms*, *TR*=1.0 *s*; Septum pellucidum and fornix (white arrow), and the internal cerebral veins (yellow arrow) are much better visualized in (c) due to the shorter echo train.

Table 1

A summary of the RFOV image performances corresponding to Figs. 2(a-e)

Images Index	FOV Reduction R_{FOV}	Field of Excitation *FOE*	Echo train length *ETL*	ETL Reduction R_{ETL}	TR_{min} *(ms)*
(a)	1	N/A	134	1	1797
(b)	2	0.8FOV	70	1.9	941
(c)	3	0.6FOV	48	2.8	644
(d)	4	0.55FOV	38	3.5	511
(e)	5	0.52FOV	32	4.2	430